ARTIFICIAL SATELLITES, Vol. 50, No. 1 – 2015
DOI: 10.1515/arsa-2015-0001

IMPACT OF THE ATMOSPHERIC DRAG ON STARLETTE, STELLA, AJISAI, AND LARES ORBITS

Krzysztof Sośnica 1,2
1 Astronomical Institute, University of Bern, Bern, Switzerland
2 Institute of Geodesy and Geoinformatics, Wroclaw University of Environmental and Life Sciences, Wroclaw, Poland
e-mail: sosnica@aiub.unibe.ch, krzysztof.sosnica@igig.up.wroc.pl

ABSTRACT. The high-quality satellite orbits of geodetic satellites, which are determined using Satellite Laser Ranging (SLR) observations, play a crucial role in providing, e.g., low-degree coefficients of the Earth's gravity field including geocenter coordinates, Earth rotation parameters, as well as the SLR station coordinates. The appropriate modeling of non-gravitational forces is essential for the orbit determination of artificial Earth satellites. The atmospheric drag is a dominating perturbing force for satellites at low altitudes up to about 700-1000 km. This article addresses the impact of the atmospheric drag on mean semi-major axes and orbital eccentricities of geodetic spherical satellites: Starlette, Stella, AJISAI, and LARES. Atmospheric drag causes the semi-major axis decays amounting to about $\Delta a = -1.2$, -12, -14, and -30 m/year for LARES, AJISAI, Starlette, and Stella, respectively. The density of the upper atmosphere strongly depends on the solar and geomagnetic activity. The atmospheric drag affects the along-track orbit component to the largest extent, and the out-of-plane to a small extent, whereas the radial component is almost unaffected by the atmospheric drag.

Keywords: Satellite Geodesy, Atmospheric Drag, SLR, Mean Orbital Elements

1. INTRODUCTION

Satellite Laser Ranging (SLR) provides substantial information about the origin of the reference frame (i.e., geocenter coordinates, Thaller et al., 2014; Sośnica et al., 2013), the scale of reference frame, and low-degree coefficients of the Earth's gravity field (Bianco et al., 1998; Cheng et al., 1997; Chen and Wilson, 2008; Cheng et al., 2013). The accuracy of laser observations at a level of a few millimeters allows deriving the high-quality orbits of geodetic satellites (Pearlman et al., 2002; Lejba and Schillak, 2011). Therefore, SLR has a remarkable potential in realizing global reference frames and providing state-of-the-art geodetic parameters.

The appropriate modeling of gravitational and non-gravitational forces is, however, a key issue for the orbit determination of low orbiting satellites and for determination of geodetic parameters based on SLR observations. The satellite perturbations of gravitation origin (e.g., due to Earth's oblateness and high-degree gravity field coefficients, solid

Earth, ocean, and atmospheric tides) strongly depend on the altitude of a satellite. Non-gravitational forces depend not only on the altitude of a satellite, but also on properties of material the satellite is made of. The accelerations caused by non-gravitational forces are usually proportional to the area-to-mass ratio coefficient, which is the ratio of the satellite's cross-section and the mass.

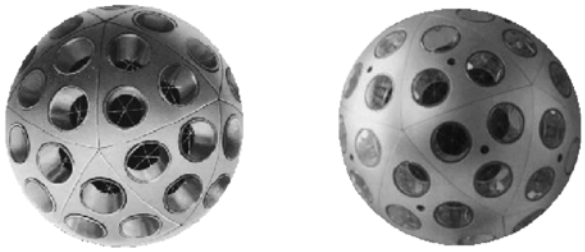

Fig. 1. Starlette (left) and Stella (right) satellites. Courtesy of CNES.

2. LOW-ORBITING GEODETIC SATELLITES

2.1. Starlette and Stella

Starlette and Stella are twin French passive geodetic satellites, launched by the Centre National d'Etudes Spatiales (CNES) in 1975 and 1993, respectively. Their cores consist of Uranium 238 formed as icosahedrons with 20 triangular planes (Seeber, 2003). Each triangle carries a spherical aluminum cap with three embedded retroreflectors (see Figure 1). The diameter of each satellite is 24 cm, and the masses are 47 kg and 48 kg for Starlette and Stella, respectively. It corresponds to the area-to-mass ratios of $9.6{\cdot}10^{-4}$ m^2kg^{-1} and $9.4{\cdot}10^{-4}$ m^2kg^{-1}, i.e., about 36% higher than for the LAGEOS satellites, which results in a somewhat higher sensitivity to non-gravitational perturbations, e.g., to solar radiation pressure. Both Stella and Starlette are equipped with 60 identical corner cube retroreflectors for SLR tracking.

The Starlette's inclination angle of about 50°, high orbital eccentricity of 0.021, and low altitude (800 km in perigee) allow determining the spherical harmonics of the Earth gravity field, especially the zonal terms due to the large drift of the ascending node and large variations of the orbital eccentricity excitation vector (Sośnica, 2014).

Stella was launched into a near-circular sun-synchronous orbit with an inclination of 98.6° and an altitude of 820 km above Earth's surface. Due to the Stella's orbit inclination angle, different than that of Starlette, a decorrelation of some parameters in combined Starlette-Stella solutions is possible (e.g., C_{20} and Length-of-Day, Sośnica et al., 2012; 2014b). Stella, along with Starlette, is mostly used for gravity field recovery, determination of the frequency dependent tidal response of the solid Earth, and the long wavelengths of the ocean tides, due to strong orbit resonances with tidal forces (Rutkowska and Jagoda, 2012).

2.2. AJISAI

AJISAI (also known as Experimental Geodetic Payload or Experimental Geodetic Satellite, EGS) was launched on August 12, 1986 by the National Space Development Agency (NASDA) currently reorganized as Japan Aerospace Exploration Agency (JAXA). Objective of the mission is the precise positioning of fiducial points on the Japanese Islands

and testing of NASDA's two-stage launch vehicle (Otsubo et al., 1994). The satellite is equipped with 1440 uncoated fused silica corner cube reflectors for SLR (see Figure 2), arranged in the form of 15 rings around the symmetry axis (Kucharski et al., 2009). AJISAI is also equipped with 318 mirrors used for the optical/CCD observations. The mirrors are used for photometric measurements of AJISAI's spin period (Otsubo et al., 2006), as well. The satellite orbits at the altitude of 1490 km and an inclination of 50°. The mass of the satellite is 685 kg and the diameter is 215 cm. The area-to-mass ratio of AJISAI ($58{\cdot}10^{-4}$ m^2kg^{-1}) is less favorable than in case of other geodetic satellites. Thus, AJISAI has a considerable sensitivity to non-gravitational forces perturbing its orbit. On the other hand, the layers of aluminum nets and a partly hollow interior minimize the magnetic torques affecting other geodetic satellites made of solid metal. AJISAI is one of the fastest spinning object amongst the geodetic satellites (Kucharski et al., 2013). Its specific construction prevents the Earth's magnetic field from inducing eddy currents in the body, hence minimizing the slowdown of its spin and stabilizing the orientation of the spacecraft.

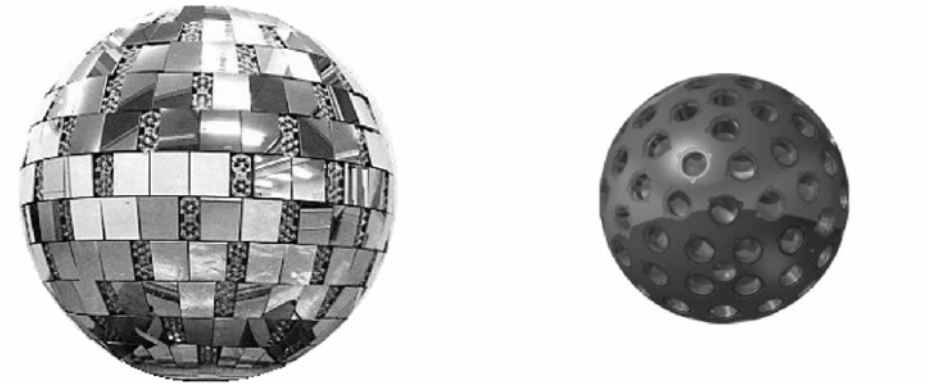

Fig. 2. AJISAI (left) and LARES (right) satellites (not to scale). Courtesy of JAXA and ASI.

2.3. LARES

LARES (LAser RElativity Satellite) was designed by the Scuola di Ingegneria Aerospaziale at the University of Rome and manufactured by the Italian Space Agency (ASI). The satellite was launched by the European Space Agency (ESA) on February 13, 2012 with the maiden flight of the new ESA small launcher VEGA. LARES was placed in a circular orbit at a height of 1450 km with an inclination of 69.5°.

This fully passive spherical satellite is made of a high density solid tungsten alloy and equipped with 92 fused silica corner cube reflectors (see Figure 2). The corner cubes are arranged in the form of 10 rings around the polar axis of the body (Kucharski et al., 2012). As opposed to the other geodetic satellites, LARES consists only of one metal layer without a specified inner core (Pavlis et al., 2012). The mass of the satellite is 386.8 kg and the satellite radius is only 18 cm. Therefore, LARES has nowadays the smallest area-to-mass ratio amongst all artificial satellites ($2.7{\cdot}10^{-4}$ m^2kg^{-1}, i.e., 2.5 times smaller than LAGEOS), and moreover, LARES is the densest object in the Solar System (Pavlis et al., 2012). Consequently, LARES is very sensitive to gravitational forces as well as to the perturbations emerging from the theory of general relativity due to its low altitude, whereas the orbit perturbations related to non-gravitational forces are greatly minimized.

The basic purpose of the satellite mission is to achieve important measurements in gravitational physics, space geodesy, and geodynamics: in particular, together with the LAGEOS-1 and LAGEOS-2 satellites and with the GRACE models, it will improve the accuracy of the determination of Earth's gravitomagnetic field, and of the Lense-Thirring effect (Pavlis et al., 2012). Besides, the satellite can be used for the gravity field determination of low-degree harmonics, estimation of Earth rotation parameters, and defining the terrestrial reference frame (Sośnica et al., 2014a).

3. PERTURBATIONS OF SATELLITE ORBITS

The most important non-gravitational forces acting on geodetic satellites can be divided into four groups:

- radiation pressure:
  - direct solar radiation pressure:
    - direct radiation,
    - umbra and penumbra radiations,
    - light aberration,
  - thermal satellite re-radiation forces:
    - the Yarkovsky effect,
    - the Yarkovsky-Schach effect,
  - Earth radiation pressure:
    - infrared emissivity radiation pressure,
    - albedo reflectivity radiation pressure,
- atmospheric drag:
  - drag due to the electrically neutral atmosphere,
  - drag due to charged particles,
- thrust due to satellite asymmetricity,
- de-spinning due to interactions with the Earth's magnetic field.

For satellites at altitudes higher than about 2000 km, e.g., for LAGEOS, the impact of atmospheric drag is negligible and the direct solar radiation pressure constitues the source of the largest perturbations.

Table 1 summarizes the forces acting on four geodetic satellites with different altitudes and different area-to-mass ratios. The impact of gravitational forces strongly depends on the satellite's altitude. The impact of Earth's oblateness term C_{20} on LAGEOS is only 9 times smaller than the impact of the same term on Starlette, whereas the impact of $C_{20\,20}$ (sectorial harmonic of degree= 20 and order= 20) on LAGEOS is already about 1000 smaller than on Starlette. Thus, using the satellites of different altitudes allows discriminating of different coefficients when the geopotential parameters are to be determined.

Comparing LARES and AJISAI, namely two satellites of similar altitudes, the impact of gravitational forces is nearly the same, whereas the impact of non-gravitational forces is about 22 times smaller for LARES than for AJISAI. The impact of non-gravitational forces

Table 1: Perturbing accelerations acting on geodetic satellites derived using the Bernese GNSS Software, after Sośnica (2014). Units of the perturbing accelerations: ms^{-2}.

	Accel. on LAGEOS-1/2	Accel. on AJISAI	Accel. on LARES	Accel. on Stella/Starlette*
Altitute [km]:	5.860/5.620	1.500	1.450	820/800-1.100
Inlination [deg]:	109.9/52.7	69.5	50.0	98.6/49.8
Mass [kg]:	407/405	685	387	48/47
Area-to-mass [m^2kg^{-1}]:	$6.9/7.0 \cdot 10^{-4}$	$58 \cdot 10^{-4}$	$2.7 \cdot 10^{-4}$	$9.4/9.6 \cdot 10^{-4}$
Gravitational perturbations:				
· Earth's monopole	2.7	6.4	6.5	7.7
· Earth's oblateness $C_{2\,0}$	$1.0 \cdot 10^{-3}$	$6.2 \cdot 10^{-3}$	$6.3 \cdot 10^{-3}$	$8.8 \cdot 10^{-3}$
· Annual variations in $C_{2\,0}$	$1.7 \cdot 10^{-10}$	$1.0 \cdot 10^{-9}$	$1.1 \cdot 10^{-9}$	$1.5 \cdot 10^{-9}$
· Low-order grav. $C_{2\,2}$	$6.0 \cdot 10^{-6}$	$3.6 \cdot 10^{-5}$	$3.7 \cdot 10^{-5}$	$5.1 \cdot 10^{-5}$
· Low-order grav. $C_{6\,6}$	$8.6 \cdot 10^{-8}$	$3.1 \cdot 10^{-6}$	$3.2 \cdot 10^{-6}$	$6.3 \cdot 10^{-6}$
· Mid-order grav. $C_{20\,20}$	$8.1 \cdot 10^{-13}$	$1.5 \cdot 10^{-8}$	$1.6 \cdot 10^{-8}$	$1.1 \cdot 10^{-7}$
· Grav. attr. of Moon	$2.1 \cdot 10^{-6}$	$1.4 \cdot 10^{-6}$	$1.4 \cdot 10^{-6}$	$1.3 \cdot 10^{-6}$
· Grav. attr. of Sun	$9.6 \cdot 10^{-7}$	$6.4 \cdot 10^{-7}$	$6.5 \cdot 10^{-7}$	$5.7 \cdot 10^{-7}$
· Grav. attr. of Venus	$1.3 \cdot 10^{-10}$	$8.5 \cdot 10^{-11}$	$8.5 \cdot 10^{-11}$	$7.8 \cdot 10^{-11}$
· Solid Earth tides	$3.7 \cdot 10^{-6}$	$2.0 \cdot 10^{-5}$	$2.0 \cdot 10^{-5}$	$2.9 \cdot 10^{-5}$
· Ocean tides	$3.7 \cdot 10^{-7}$	$1.9 \cdot 10^{-6}$	$2.0 \cdot 10^{-6}$	$3.0 \cdot 10^{-6}$
General relativity:				
· Schwarzschild effect	$2.8 \cdot 10^{-9}$	$1.1 \cdot 10^{-8}$	$1.1 \cdot 10^{-8}$	$1.4 \cdot 10^{-8}$
· Lense-Thirring effect	$2.7 \cdot 10^{-11}$	$1.3 \cdot 10^{-10}$	$1.4 \cdot 10^{-10}$	$1.8 \cdot 10^{-10}$
· Geodetic precession	$3.4 \cdot 10^{-11}$	$4.2 \cdot 10^{-11}$	$4.2 \cdot 10^{-11}$	$4.3 \cdot 10^{-11}$
Non-gravitational perturbations:				
· Solar radiation pressure	$3.5 \cdot 10^{-9}$	$2.5 \cdot 10^{-8}$	$1.1 \cdot 10^{-9}$	$4.4 \cdot 10^{-9}$
· Earth radiation pressure	$4.4 \cdot 10^{-10}$	$8.6 \cdot 10^{-9}$	$3.9 \cdot 10^{-10}$	$1.8 \cdot 10^{-9}$
· Thermal re-radiation	$5.0 \cdot 10^{-11}$	$4.1 \cdot 10^{-10}$	$1.9 \cdot 10^{-11}$	$6.9 \cdot 10^{-11}$
· Light aberration	$1.1 \cdot 10^{-13}$	$1.1 \cdot 10^{-12}$	$5.1 \cdot 10^{-14}$	$2.0 \cdot 10^{-13}$
· Atmospheric drag ($\sim$ min)	$0.8 \cdot 10^{-14}$	$3.0 \cdot 10^{-11}$	$2.6 \cdot 10^{-12}$	$5.0 \cdot 10^{-11}$
· Atmospheric drag ($\sim$ max)	$2.0 \cdot 10^{-13}$	$5.9 \cdot 10^{-10}$	$4.8 \cdot 10^{-11}$	$5.0 \cdot 10^{-8}$

*in perigee

strongly depends on the area-to-mass ratio ($58.0 \cdot 10^{-4}$ for AJISAI and $2.7 \cdot 10^{-4}$ m^2 kg^{-1} for LARES). The impact of the direct solar radiation pressure on LAGEOS and Starlette/Stella is, thus, similar, because of comparable area-to-mass ratios, despite a totally different impact of the Earth's gravity field. For Stella and Starlette the variations of minimum and maximum values of the atmospheric drag can reach even three orders of magnitudes. Besides the thermal effects and atmospheric drag, geodetic satellites are affected by the light aberration effect, causing a secular decay of satellites' semi-major axes of the order of 8, 7, 43, and 2 mm/year for LAGEOS, Starlette (Stella), AJISAI, and LARES, respectively (Beutler, 2005). The light aberration effect is, however, much smaller than the thermal and atmospheric drags, and thus, it has never been directly observed, so far.

3.1. ATMOSPHERIC DRAG

The drag due to the neutral and charged atmosphere particles is a dominating dissipative force for low orbiting satellites. The atmospheric drag leads to a loss of energy in a sense represented by a reduction of the satellite's semi-major axis a.

The upper atmosphere consists of the thermosphere beginning at the altitude of 95-120 km and the exosphere beginning at the altitude of 500-1000 km. The boundaries between the layers vary depending on solar activity, but in general, the low geodetic satellites orbit in the exosphere for most of the time. The major gases in the Earth's upper atmosphere are the lightest atmospheric gases, mainly: hydrogen, helium, and atomic oxygen. In the exosphere, there are negligible atomic and molecular collisions between the particles and the constituent atoms are on purely ballistic trajectories.

Assuming the laminar air currents, and that the atmosphere is co-rotating with the Earth, and neglecting thermal motion of molecules, the acceleration due to the atmospheric drag can be expressed as (Beutler, 2005):

$$\mathbf{a}_D = -\frac{C_D}{2}\,\rho_{(h,T,\lambda,\phi,F_{10.7},A_p)}\,\frac{A}{m}\,\dot{r}'^2\,\frac{\dot{\mathbf{r}}'}{|\dot{r}'|}, \tag{1}$$

where:

- C_D - scaling factor (C_D=2 for spherical satellites and unbiased atmospheric density models),
- $\rho_{(h,T,\lambda,\phi,F_{10.7},A_p)}$ - density of the atmosphere,
- $\frac{A}{m}$ - area-to-mass (cross-section-to-mass) ratio,
- $\dot{\mathbf{r}}'$ - a relative velocity of the satellite with respect to the rotating atmosphere.

The density of the atmosphere ρ is a complex function of many constituents. E.g., the MSISe-90 (Mass Spectrometer and Incoherent Scatter extended) model (Hedin, 1991) and its successor NRLMSIS-00 (Picone et al., 2002), the empirical atmospheric density models, allow estimating the atmospheric density as a function of:

- h - the height above the Earth's surface,
- T - time of the day (solar time) and the day of the year,
- λ, ϕ - geographical longitude and latitude,

- $F_{10.7}$ - solar flux (penticton 2800 MHz corresponding to 10.7 cm),
- A_p - geomagnetic index.

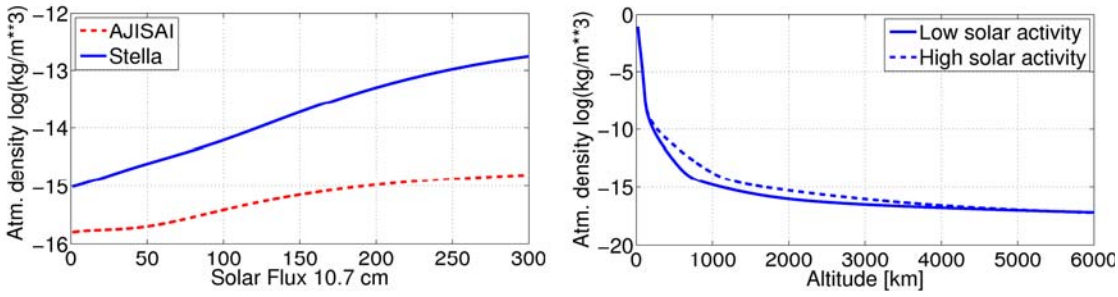

Fig. 3. Left: Atmospheric density as a function of solar flux index $F_{10.7}$ for the altitude of Stella and AJISAI according to the NRLMSIS-00 model.
Right: Relation between the atmospheric density and the satellite altitude for low solar activity ($F_{10.7}$=80 and A_p=15) and high solar activity ($F_{10.7}$=250 and A_p=40) according to the NRLMSIS-00 model.

3.2. DENSITY OF THE UPPER ATMOSPHERE

Figure 3, left shows the atmospheric density as a function of the solar flux index $F_{10.7}$ for the orbit altitudes of Stella (or of Starlette in perigee) and AJISAI from the NRLMSIS-00 model. The atmospheric density at the LARES' altitude is similar to that at the AJISAI's. The solar flux index $F_{10.7}$ depends on the phase of the 11-year cycle of solar activity. The figure shows that the difference of atmospheric density, only due to the solar activity, varies within two orders of magnitude for Stella's altitude. During the periods of low solar activity the density is about $2 \cdot 10^{-15}$ kg m^{-3}, whereas during the high solar activity the density is $2 \cdot 10^{-13}$ kg m^{-3} for Stella's altitude. The variations of atmospheric density for AJISAI's altitude are smaller, yielding one order of magnitude.

Figure 3, right shows the relationship between the atmospheric density from the NRLMSIS-00 model and the altitude of a satellite for the low and high solar activities. The figure shows that the density at the altitude 900 km is about 10^{-14} kg m^{-3} during high solar activities. For the area-to-mass ratio ($\frac{A}{m}$) of Starlette or Stella, the acceleration due to the atmospheric drag at this altitude would be $6 \cdot 10^{-10}$ ms^{-2}, i.e., about five times smaller than the acceleration due to the direct solar radiation pressure (see Table 1). But 100 km lower, i.e., at 800 km the impact of both non-gravitational forces is already comparable and the induced acceleration yields $34 \cdot 10^{-10}$ ms^{-2}.

Sośnica (2014) demonstrated that the Yarkovsky effect imposes an acceleration on LAGEOS of about $5 \cdot 10^{-12}$ ms^{-2}. A similar acceleration due to atmospheric drag would be at an altitude of 2500-4000 km depending on the solar activity. At the altitude of LAGEOS, the drag is mostly due to the interactions with the Van Allen belt particles. High and low orbiting geodetic satellites pass through Van Allen radiation belts, which are layers of energetic charged particles that are held in place around the Earth by its magnetic field. Spherical satellites absorb the van Allen belt particles that pass through, and change their momentum as a result. The interactions with charged particles cause a small drag-like force even at the LAGEOS altitudes (Rubincam, 1986).

It should be noted that the atmospheric density is almost independent of solar activity below the altitude of 150 km. The maximum variations of density are at the altitudes of about 800 km, where most of the geodetic SLR satellites are orbiting, e.g., Starlette, Stella, Westpack, Larets, BLITS.

Figure 4, top shows the time series of a priori $F_{10.7}$ and A_p indices. The values of $F_{10.7}$ reach their maximum during the high solar activity periods (2000-2004 and after 2011), whereas the geomagnetic A_p index shows a small delay with respect to the solar activity. $F_{10.7}$ and A_p are used in the development version of the Bernese GNSS Software (Dach et al., 2007) as the a priori values for the atmospheric drag computation. The $F_{10.7}$ and A_p indices are scaling factors of the atmospheric density models. They are, however, non-linear scaling factors as shown in the Figures 3, right and 4, bottom. Figure 4, bottom also shows the dominating impact of the $F_{10.7}$ index on the estimated air density. The variations of the air density due to A_p are much smaller and they do not exceed 10% of the impact of the $F_{10.7}$ index.

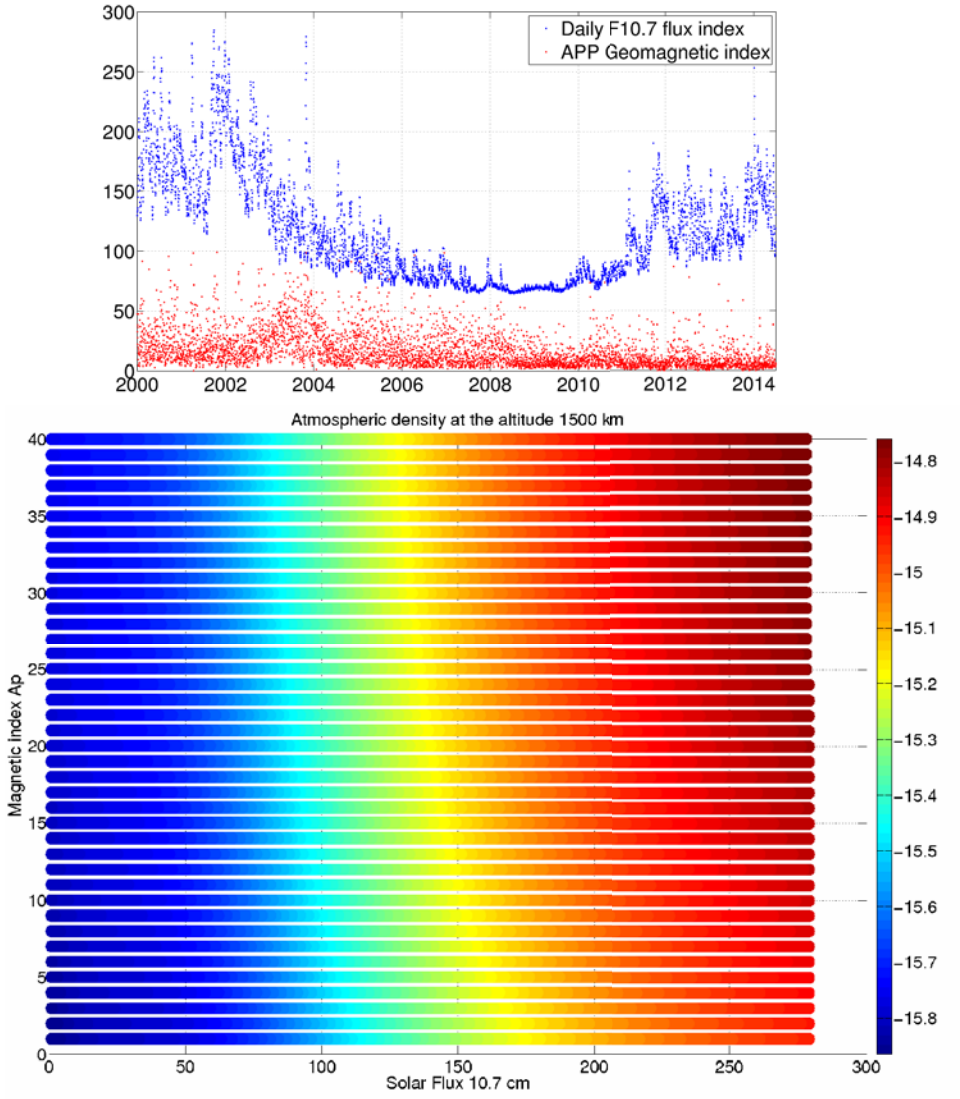

Fig. 4. Top: Time series of the solar flux $F_{10.7}$ and Geomagnetic indices A_p. **Bottom:** Atmospheric density as a function of the solar flux index $F_{10.7}$ and geomagnetic index A_p for the orbital altitude of AJISAI. Units: log(kg m^{-3}).

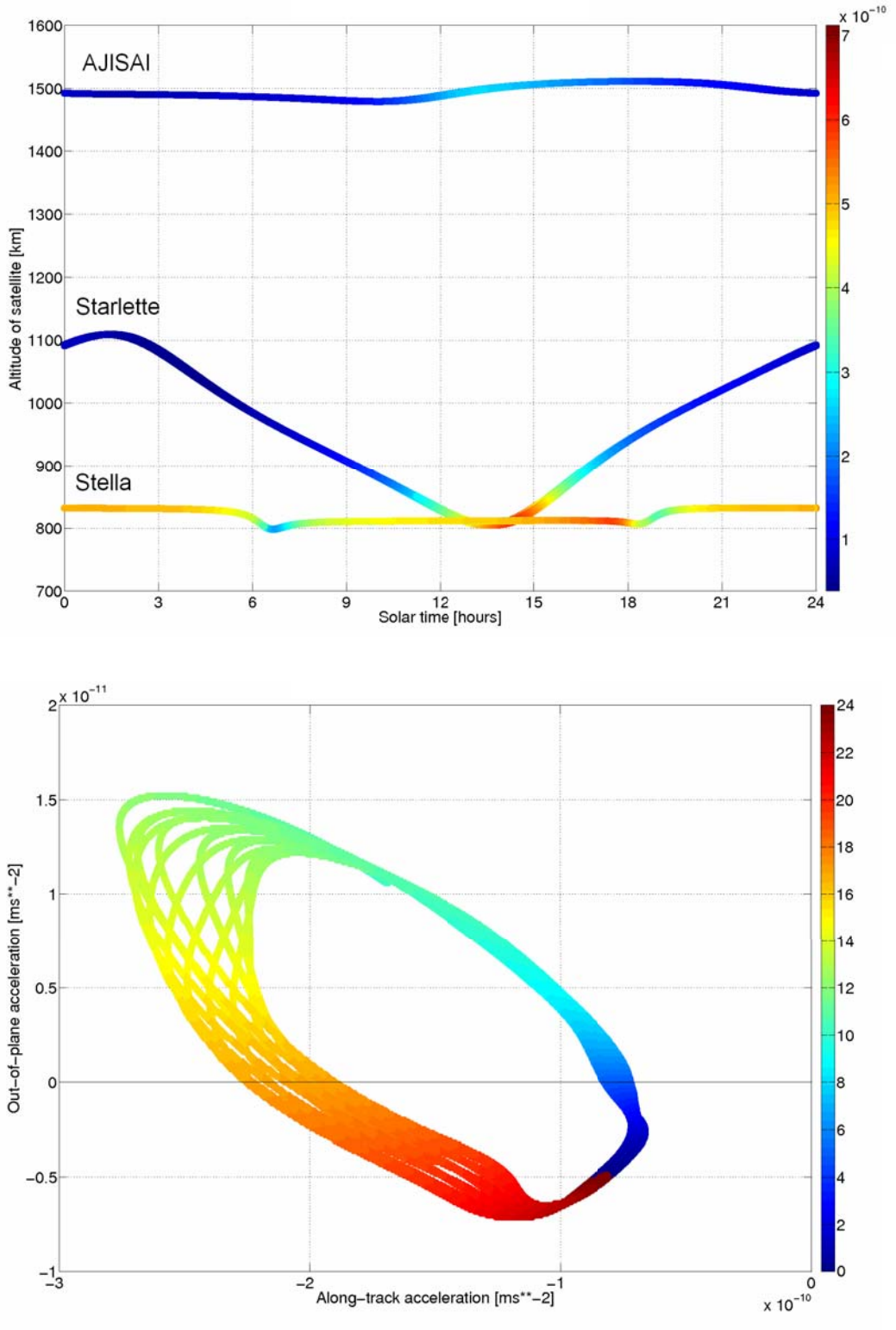

Fig. 5. Top: Total acceleration acting on low geodetic satellites due to atmospheric drag for July 30, 2003 (a period with a moderate solar activity but with an increased geomagnetic activity). Units: ms^{-2}.
Bottom: Acceleration acting on AJISAI due to atmospheric drag in the along-track and out-of-plane directions as a function of solar time. Units of the colorbar: hours. Note different scales for X- and Y axes.

4. IMPACT ON SATELLITE ORBITS

Figure 5, top shows the estimated acceleration on Stella, Starlette, and AJISAI due to the atmospheric drag for one day July 30, 2003, as a function of solar time. In case of Starlette, having large orbital eccentricity, the maximum accelerations are during the periods when the altitude of the satellite is minimum (812 km). In Starlette's apogee (1120 km) the acceleration is one order of magnitude smaller than in the perigee.

For satellites having almost circular orbits (AJISAI and Stella) there is no direct relationship between the altitude and the acceleration due to the atmospheric density. The variations of the accelerations are much smaller for these satellites as compared to Starlette. In case of AJISAI the acceleration depends on the solar time. In case of Stella the acceleration is more a function of the actual geographical position and the relative velocity w.r.t. the rotating atmosphere. The acceleration on Stella is similar to the maximum acceleration on Starlette in the perigee. The acceleration on Starlette in apogee is, however, even smaller than the minimum acceleration on AJISAI, despite much higher altitude of AJISAI. It is because of the larger area-to-mass ratio of AJISAI, which makes this satellite very sensitive to non-gravitational forces.

Figure 5, bottom shows the relation between the solar time and the accelerations in along-track (S) and out-of-plane (W) for AJISAI for one day (note different scales for the X and Y axes). The acceleration in S is always negative, whereas the acceleration in W is negative or positive, but for most of the time the acceleration in W is positive. The maximum (negative) acceleration in S and maximum positive acceleration in W is between 12h and 14h of the solar time. The zero acceleration in W is at around 6h and 16h. The minimum acceleration in S is around 2h, whereas the maximum negative acceleration in the W at about 21h. The figure shows that the relations between the accelerations in different orbit directions are not straightforward.

If a satellite's velocity vector were always perpendicular to the layers formed by non-rotating atmospheric particles, the drag force would affect only the tangential ($\sim$along-track) orbit direction. Because the atmosphere co-rotates with the Earth and the satellites have different orbit inclination angles (and thus different directions of velocity vectors w.r.t. the atmosphere), the atmospheric drag affects not only the S orbital direction, but also W and radial R.

Figures 6, top and 6, bottom show the accelerations in S and W due to the atmospheric drag for Starlette and AJISAI projected on the Earth's surface. The acceleration in S is always negative. The acceleration in W is about twenty times smaller than the acceleration in S for both, Starlette and AJISAI, and it may assume positive or negative values. The accelerations in R are of the order of 10^{-13} ms^{-2}, and therefore they are negligible.

In Figures 6, top and 6, bottom the dependency between the acceleration on ascending satellites (moving towards north-east) and descending satellites (moving towards south-east) is apparent. The dependency in S can be explained by the Starlette's orbital eccentricity. This cannot, however, explain the dependency in W on AJISAI, because the eccentricity of AJISAI's orbit is very small. The dependency in W on AJISAI can, however, be explained by the relative velocity between the satellite and the rotating atmosphere.

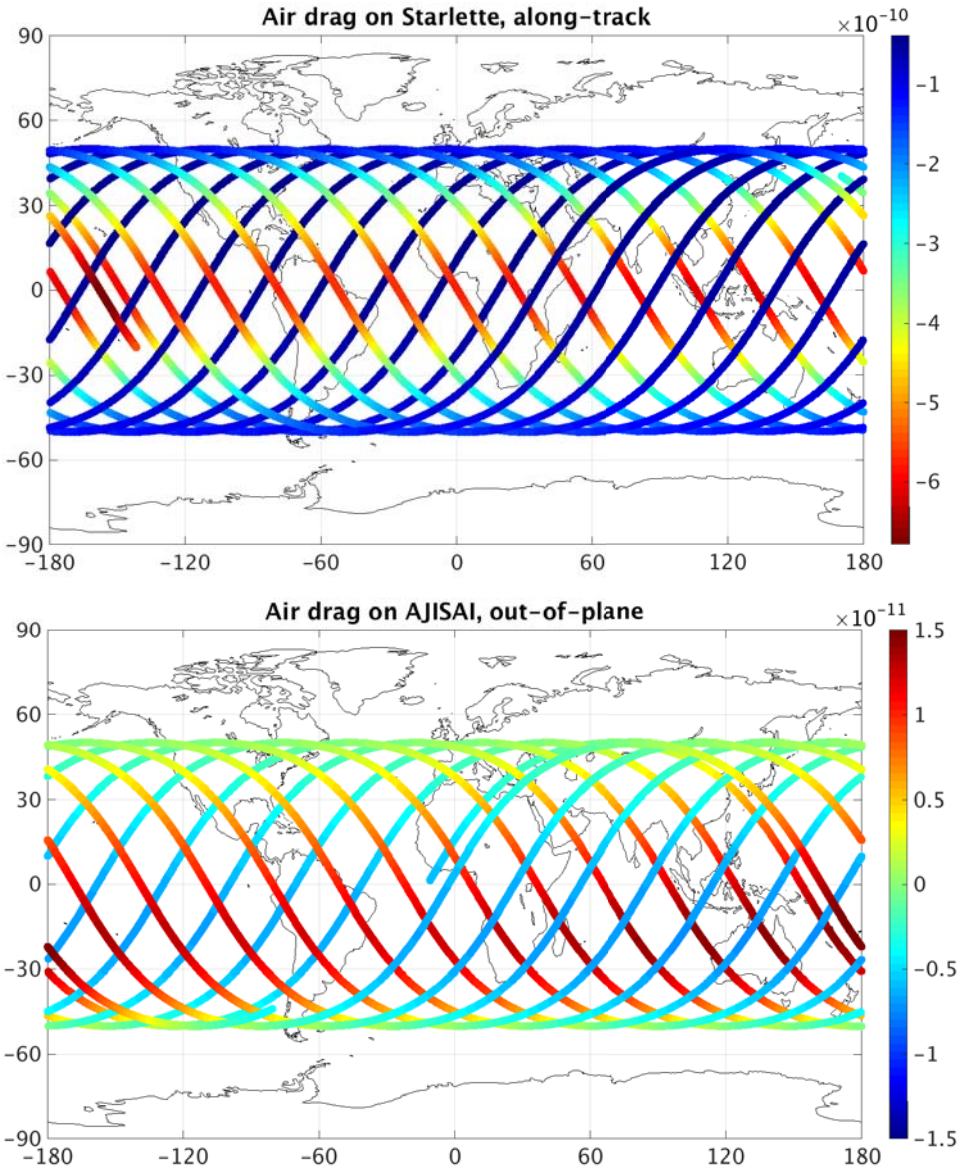

Fig. 6. Acceleration on Starlette and AJISAI due to atmospheric drag for the **Top:** along-track, and **Bottom:** out-of-plane directions. Units: ms^{-2}.

The relative velocity depends on the inclination angle and the altitude of a satellite's orbit. For satellites with the orbit inclination angle $0° < i < 90°$ the angle between the relative velocity vector and the normal vector to orbital plane W is above 90° when a satellite is ascending. This implies negative accelerations in W due to atmospheric drag for ascending satellites. On the other hand, during the satellite's descending period, the angle between the relative velocity and the normal to the orbital plane is small, implying that the large positive accelerations occur in the out-of-plane direction.

5. MEAN ORBITAL ELEMENTS

Osculating orbital elements $\mathbf{I}(t)$, derived from the series of satellite's state vectors $\mathbf{r}(t), \dot{\mathbf{r}}(t)$, show large high-frequency variations. Calculating the mean orbital elements, which allow us to study the long-term evolution of orbital elements, is necessary in order to study

secular orbit perturbations of the order of several cm/year. The mean elements are computed by averaging the osculating elements over a number of full revolutions (Beutler, 2005). A set of mean elements:

$$\bar{\mathbf{I}}(t) = \left\{ \bar{a}(t), \bar{e}(t), \bar{i}(t), \bar{\Omega}(t), \bar{\omega}(t), \bar{u}_0(t) \right\}, \tag{2}$$

is obtained by:

$$\bar{\mathbf{I}}(t, \Delta t(t)) = \frac{1}{\Delta t} \int_{t-\Delta t/2}^{t+\Delta t/2} \mathbf{I}(t') dt', \tag{3}$$

where $\Delta t(t)$ denotes the averaging time interval covering an entire number of revolution periods and $\mathbf{I}(t)$ is a set of orbital elements associated with an epoch t:

$$\mathbf{I}(t) = \left\{ a(t), e(t), i(t), \Omega(t), \omega(t), u_0(t) \right\}. \tag{4}$$

To study the impact of the atmospheric drag on low orbiting satellites, we processed 10 years of SLR data of Starlette, Stella, and AJISAI for the time span 2002.0-2012.0 and 2.3 years of LARES data (2012.2-2014.5), and then we transform the derived osculating elements to the mean orbital elements by averaging the osculating orbital elements with the 0.1 s interval over 12 revolutions.

The solutions are computed using the development version of the Bernese GNSS Software with the capability of processing SLR observations to low orbiting geodetic satellites. For the orbit integration the collocation method developed by Beutler (2005) is used with a 1-minute interval step and using a polynomial degree 12. The variational equations of the equation of motion are calculated in 4-minute intervals using degree 12 polynomial. 1-day satellite arcs are generated on the basis of SLR observations provided by the global network of the SLR stations. The orbit modeling standards follow the Conventions of the International Earth Rotation Service (IERS) from 2010 (Petit and Luzum, 2010) and the recommendations of the International Laser Ranging Service (ILRS) Analysis Working Group for SLR data exclusions and station corrections. Besides the 6 Keplerian elements, the orbital arc definition includes once-per-revolution empirical accelerations in S and W and the estimation of the atmospheric drag scaling factor C_D with the 1-day interval. More details on the orbit modeling standards for low orbiting geodetic satellites can be found in Sośnica et al., (2014b).

In the final step, the orbital osculating elements are represented with the 0.1 s intervals and then, they are averaged out over 12 revolutions to obtain the values of the mean orbital elements.

5.1 STARLETTE, STELLA, AND AJISAI

Figure 7 shows the mean semi-major axes of AJISAI, Starlette, and Stella, respectively, with fitted polynomial of third degree. The mean secular decays of semi-major axes yield:

- $\Delta a = -12$ m/year for AJISAI,
- $\Delta a = -14$ m/year for Starlette,
- $\Delta a = -30$ m/year for Stella.

Despite the much higher altitude of AJISAI, the secular decay due to the atmospheric drag is comparable to the secular decay of Starlette, because of different area-to-mass ratios.

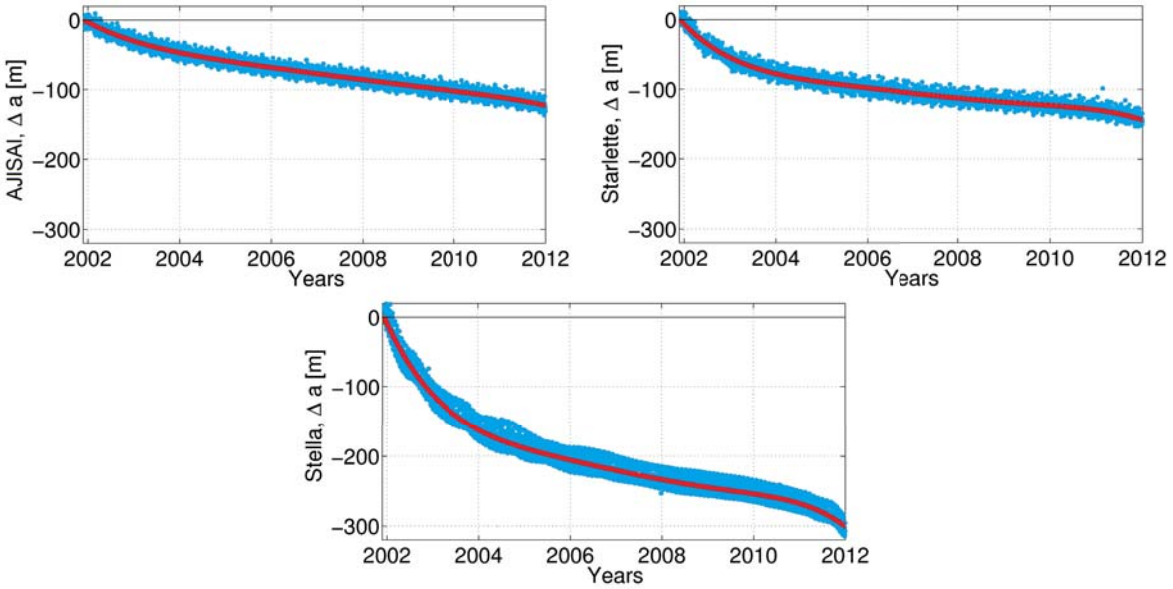

Fig. 7. Secular decay of mean semi-major axis of AJISAI, Starlette, and Stella.

The decay strongly depends on the solar activity. In 2002-2005 and in 2011 the decays of semi-major axes reach maximum, which is in particular remarkable for Starlette and Stella. Comparing the similar secular decays of AJISAI and Starlette, it turns out that the mean decay during the low solar activity (2005-2010) for AJISAI is larger (−9 m/year) than for Starlette (−7 m/year). It means that the decay of AJISAI is less dependent on the solar activity and it is more linear in time. The mean decay of Starlette is larger than the decay of AJISAI during the high solar activity periods, but lower during the low solar activity. Bezdek and Vokrouhlicky (2004) found a mean decay of Starlette's semi major axis of about $\Delta a = -30$ m/year from a 20-year analysis of the secular decay of geodetic satellites. However, in the considered period (1984-2003) two maxima of solar activity occurred which increased the orbital decay, whereas in the period considered in this paper the low solar activity is dominating.

The theoretical decay of the semi-major axis derived by Beutler (2005) yields:

$$\Delta a/\text{year} = -31557600\, n\, C_D \frac{A}{m} a^2 \rho_{(h,T,\lambda,\phi,F_{10.7},A_p)} \tag{5}$$

However, the large variations of the air density do not allow deriving an exact ρ value using just the theoretical considerations. Beutler (2005) derived also an approximated relation between the drift of a satellite eccentricity and semi-major axis, which reads as:

$$\Delta e(t) \approx \frac{\Delta a(t)}{a}. \tag{6}$$

Indeed, besides the variations with the periods equal to perigee drifts (see Figure 8), the orbital eccentricity exhibits a secular drift, and thus, the orbits become more 'circular'. The secular drift of orbital eccentricity is $1.8{\cdot}10^{-6}$/year, $2.2{\cdot}10^{-6}$/year, and $2.1{\cdot}10^{-6}$/year, for AJISAI, Starlette, and Stella, respectively. Therefore, the estimated secular drift of eccentricity agrees very well with the theory for AJISAI and Starlette. For Stella the estimated drift is 2.5 times smaller than the drift according to the approximated equation. It shows that the approximation is not fully appropriate for nearly-circular orbits.

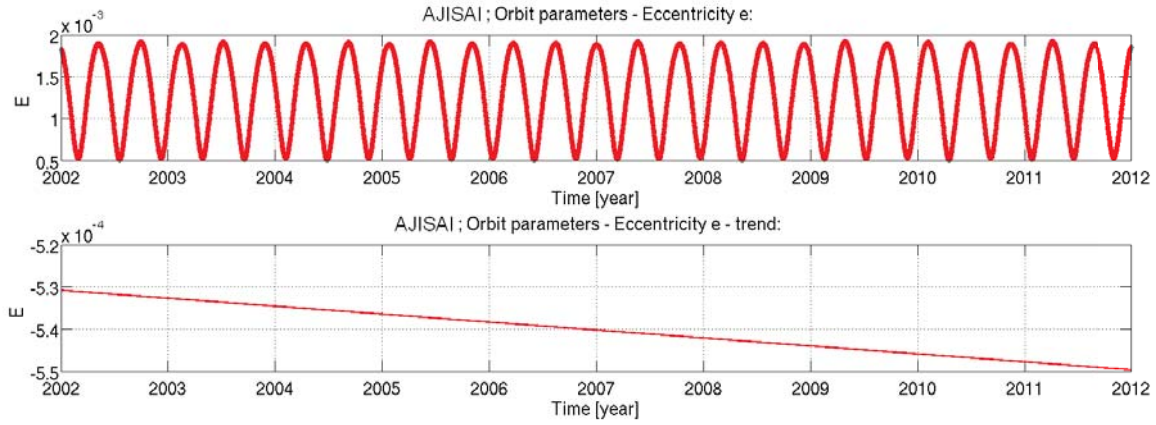

Fig. 8. Time series of mean orbital eccentricity and the secular decay of the orbital eccentricity for AJISAI.

5.2 LARES

LARES was launched in February 2012, thus, the period of the available SLR observations is shorter than for other spherical satellites. Figure 9 shows the decay of semi-major axis with a rate of about $\Delta a = -1.17$ m/year. However, between 2012 and 2014 an increased solar activity takes place, thus, the secular decay based on a long-term analysis should be roughly 30% smaller, amounting to about $\Delta a = -0.8$ m/year. Sośnica et al. (2014a) found a secular decay of LARES of $\Delta a = -0.78$ m/year from the analysis of the first months of LARES data. This discrepancy clearly indicates that an analysis for a longer period of data is necessary in order to obtain a credible value of the semi-major axis decay. The time span should include both, the periods of the high, as well as the low solar activity.

The secular decay of LARES eccentricity equals $0.2 \cdot 10^{-6}$/year. However, for a reliable assessment of this value, an analysis of a longer time span is needed, as well.

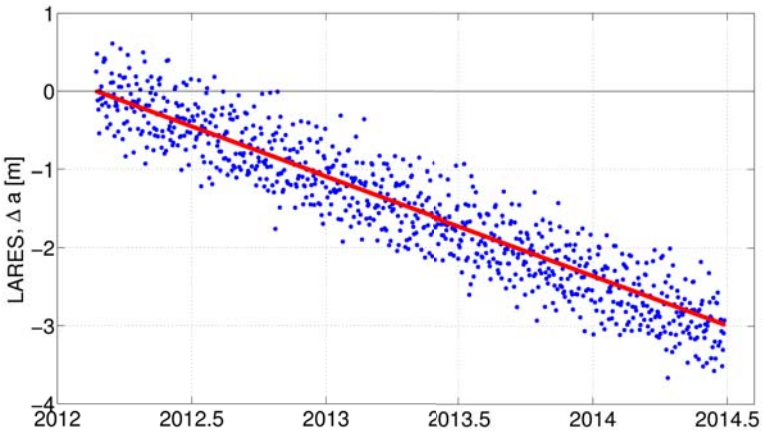

Fig. 9. Secular decay of mean semi-major axis of LARES.

6. CONCLUSIONS

The density of the upper atmosphere strongly depends on the solar and geomagnetic activity. The $F_{10.7}$ and A_p indices are scaling factors of the atmospheric density models. They are, however, non-linear scaling factors amongst which $F_{10.7}$ has the dominating impact on the density of the upper atmosphere. The variations of the air density due to A_p are much smaller and they do not exceed 10% of the impact of the $F_{10.7}$ index. The atmospheric density is almost independent of solar activity below the altitude of 150 km and above 5000 km. The maximum variations of density are at the altitudes of about 700-900 km, where most of the geodetic SLR satellites orbit the Earth, e.g., Starlette, Stella, Westpack, Larets, BLITS, and Beacon-C.

The atmospheric drag affects the S orbit component to the largest extent, and the W to a small extent (about 20x less than S). The R component is virtually unaffected by the atmospheric drag.

Atmospheric drag causes the semi-major axis decay of low orbiting satellites. The mean orbital decay from a 2.3-year analysis of LARES data and a 10 year analysis of AJISAI, Starlette, and Stella data amounts to about $\Delta a = -1.17$ m/year, $\Delta a = -12$ m/year, $\Delta a = -14$ m/year, and $\Delta a = -30$ m/year for LARES, AJISAI, Starlette, and Stella, respectively. Atmospheric drag causes as well a reduction of the orbital eccentricity and, thus, the satellite orbits become more 'circular'. The secular drift of orbital eccentricity is $0.2 \cdot 10^{-6}$/year, $1.8 \cdot 10^{-6}$/year, $2.2 \cdot 10^{-6}$/year, and $2.1 \cdot 10^{-6}$/year, for LARES, AJISAI, Starlette, and Stella, respectively. However, for a reliable assessment of LARES' secular decays, an analysis of a longer time span is needed as the secular decays strongly depend on the solar and geomagnetic activity. The mean decay during the low solar activity (2005-2010) for AJISAI is larger (-9 m/year) than for Starlette (-7 m/year), despite a much higher altitude of AJISAI. This effect is related to a much larger area-to-mass ratio of AJISAI and as a result a much larger sensitivity to non-gravitational orbit perturbations as compared to other spherical geodetic satellites. The larger AJISAI's decay than that of Starlette during low solar activity implies that the decay of AJISAI is less dependent on the solar activity and it is more linear in time. The mean decay of Starlette is larger than the decay of AJISAI during the high solar activity periods (up to -60 m/year and -20 m/year for Starlette and AJISAI, respectively), but lower during periods of the low solar activity.

The perturbations of the LARES orbits due to the atmospheric drag are up to about $4.8 \cdot 10^{-11}$ in the S orbital component, $2.6 \cdot 10^{-12}$ in W, and below $1.0 \cdot 10^{-14}$ ms^{-2} in R. The Lense-Thirring effect introduces an acceleration on LARES of about $1.4 \cdot 10^{-10}$ ms^{-2}, but only in the W and R directions. However, both the atmospheric drag and the Lense-Thirring effect introduce the once-per-revolution-like perturbations on the satellite orbits in W (Hugentobler 2008; Iorio 2008). Thus, the proper modeling of the atmospheric drag is indispensable for the confirmation of the Lense-Thirring effect with the accuracy below 1% using LARES, as the periodic orbit perturbations in W caused by the atmospheric drag during high solar activity periods correspond to about 1.9% of the perturbations caused by the Lense-Thirring effect.

Acknowledgments
The ILRS (Pearlman et al., 2002) is acknowledged for providing SLR data. SLR stations are acknowledged for a continuous tracking of geodetic satellites.

REFERENCES

Beutler G. (2005) *Methods of Celestial Mechanics*, Springer-Verlag, Berlin, Heidelberg, New York.

Bezdek A., Vokrouhlicky D. (2004) Semianalytic theory of motion for close-Earth spherical satellites includingdragand gravitational perturbations, *Planetary and Space Science* Vol. 52, No. 1233-1249.

Bianco G., Devoti R., Fermi M., Luceri V., Rutigliano P., Sciarretta C. (1998) Estimation of low degree geopotential coefficients using SLR data, *Planetary and Space Science* Vol. 46, No. 11-12, 1633-1638.

Chen J., Wilson C. (2008) Low degree gravity changes from GRACE, Earth rotation, geophysical models, and satellite laser ranging, *Journal of Geophysical Research* , Vol. 113, No. B06, 402.

Cheng M. K., Shum C., Tapley B. D. (1997) Determination of long-term changes in the Earth's gravity field from Satellite Laser Ranging observations, *Journal of Geophysical Research*, Vol. 102, No. B10, 22,377-22,390.

Cheng M., Tapley B., Ries J. (2013) Deceleration in the Earth's oblateness, *Journal of Geophysical Research* Vol. 118, 740-747.

Dach R., Beutler G., Bock H., Fridez P., Gäde A., Hugentobler U., Jäggi A., Meindl M., Mervart L., Prange L., Schaer S., Springer T., Urschl C., Walser P. (2007) *Bernese GPS Software Version 5.0*, Astronomical Institute, University of Bern, Bern, Switzerland.

Hedin A. E. (1991) Extension of the MSIS Thermosphere Model into the Middle and Lower Atmosphere, *Journal of Geophysical Research*, Vol. 96, No. A2, 1159-1172.

Hugentobler U. (2008) Orbit perturbations due to relativistic corrections. URL: `ftp://tai.bipm.org/iers/conv2010/convupdt/chapter10/add_info/relativity_hu.pdf`

Iorio I. (2008) On the impact of the atmospheric drag on the LARES mission, *Acta Physica Polonica,* B41:753-765,2010, arXiv:0809.3564 [gr-qc].

Kucharski D., Kirchner G., Otsubo T., Koidl F. (2009) 22 Years of AJISAI spin period determination from standard SLR and kHz SLR data, *Advances in Space Research* , Vol. 44, No.5, 62-626.

Kucharski D., Otsubo T., Kirchner G., Bianco G. (2012) Spin rate and spin axis orientation of LARES spectrally determined from Satellite Laser Ranging data, *Advances in Space Research,*Vol. 50, No. 11, 473-477.

Kucharski D., Schillak S., Lim H., Otsubo T. (2013) Spectral analysis of Borowiec SLR data for spin determination of geodetic satellite EGP, *Artificial Satellites* Vol. 48, No. 1, 15-23.

Lejba P., Schillak S. (2011) Determination of station positions and velocities from laser ranging observations to Ajisai, Starlette and Stella satellites, *Advances in Space Research* Vol. 47, No. 4, 654–662.

Otsubo T., Kunimori H., Engelkemier B. (1994) Ajisai Tracking Campaign SLR Japan '94 Results, *In: Symposium on Western Pacific Satellite Laser Ranging Network, Proc. of the 9th International Workshop on Laser Ranging Instrumentation,* Australian Government Publishing Service, Canberra.

Otsubo T., Kunimori H., Gotoh T. (2006) New application for khz laser ranging: Time transfer via Ajisai, *In: 15th International Laser Ranging Workshop,* Canberra, 17 Oct 2006.

Pavlis E., Ciufolni I., Paolozzi A. (2012) LARES: A new ASI mission to improve the measurement of Lense-Thirring effect with satellite laser ranging, *In: Proceedings of the Journees 2011 Systemes de reference spatio-temporels*, 19-21 September 2011 - Vienna, Austria.

Pearlman M., Degnan J., Bosworth J. (2002) The International Laser Ranging Service, *Advances in Space Research,* Vol 30, No. 2, 135-143.

Petit G., Luzum B. (2010) IERS Conventions (2010), *IERS Technical Note 36,* Frankfurt am Main: Verlag des Bundesamts fuer Kartographie und Geodaesie, ISBN 3-89888-989-6

Picone J., Hedin A., Drob D., Aikin A. (2002) NRLMSISE-00 empirical model of the atmosphere: Statistical comparisons and scientific issues, *Journal of Geophysical Research* Vol. 107, No. A12, 1468.

Rubincam D. (1987) LAGEOS Orbit Decay Due to Infrared Radiation From Earth, *Journal of Geophysical Research* Vol. 92, 1287-1294.

Rutkowska M., Jagoda M. (2012) Estimation of the elastic earth parameters using SLR data for the low satellites STARLETTE and STELLA, *Acta Geophysica* Vol. 60, No. 4, DOI 10.2478/s11600-012-0045-5.

Seeber G. (2003) *Satellite Geodesy*, 2nd edn. de Gruyter.

Sośnica K., Thaller D., Jäggi A., Dach R., Beutler G. (2012) Sensitivity of Lageos Orbits to Global Gravity Field Models, *Artificial Satelllites* Vol. 47, No. 2, 47-65, DOI 10.2478/v10018-012-0013-y.

Sośnica K., Thaller D., Dach R., Jäggi A., Beutler G. (2013) Impact of loading displacements on SLR-derived parameters and on the consistency between GNSS and SLR results, *Journal of Geodesy* Vol. 87, No. 8, 751–769, DOI 10.1007/s00190-013-0644-1.

Sośnica K. (2014) *Determination of Precise Satellite Orbits and Geodetic Parameters using Satellite Laser Ranging,* PhD thesis of the Faculty of Science of the University of Bern, ISBN: 978-83-938898-0-8.

Sośnica K., Baumann C., Thaller D., Jäggi A., Dach R. (2014a) Combined LARES-LAGEOS solutions, *In: Proceedings of the 18th International Workshop on Laser Ranging* 11-15 November 2013 Fujiyoshida, Japan.

Sośnica K., Jäggi A., Thaller D., Dach R., Beutler G. (2014b) Contribution of Starlette, Stella, and AJISAI to the SLR-derived global reference frame, *Journal of Geodesy* Vol. 88, No. 8, 789-804, DOI 10.1007/s00190-014-0722-z.

Thaller D., Sośnica K., Dach R., Jäggi A., Beutler G., Mareyen M., Richter B. (2014) Geocenter coordinates from GNSS and combined GNSS-SLR solutions using satellite co-locations, *In: Earth on the Edge: Science for a Sustainable Planet, International Association of Geodesy Symposia,* Vol. 139, 129-134, DOI 10.1007/978-3-642-37222-3 16.

Received: 2014-10-20,
Reviewed: 2015-02-07, by David A. Vallado, and 2015-02-09, by Daniela Thaller,
Accepted: 2015-03-05.